




Crystal structure of fluvoxamine maleate, (C₁₅H₂₂F₃N₂O₂)(HC₄H₂O₄)

James Kaduk^{1,2} , Anja Dosen³  and Tom Blanton³ ¹Illinois Institute of Technology, Department of Chemistry, Chicago, IL, USA²North Central College, Department of Physics, Naperville, IL, USA³International Centre for Diffraction Data (ICDD), Newtown Square, PA, USA

(Received 12 April 2025; revised 25 October 2025; accepted 27 October 2025)

Abstract: The crystal structure of fluvoxamine hydrogen maleate has been solved and refined using synchrotron X-ray powder diffraction data and optimized using density functional theory techniques. Fluvoxamine maleate crystallizes in space group $P2_1/c$ (#14) with $a = 21.6310(15)$, $b = 5.3180(4)$, $c = 19.5555(15)$ Å, $\beta = 99.979(5)^\circ$, $V = 2,215.48(25)$ Å³, and $Z = 4$ at 298 K. The crystal structure consists of alternating double layers of cations and anions parallel to the bc -plane. Hydrogen bonds link the layers of anions and cations parallel to the bc -plane. The powder pattern has been submitted to the International Centre for Diffraction Data for inclusion in the Powder Diffraction FileTM (PDF[®]). © The Author(s), 2025. Published by Cambridge University Press on behalf of International Centre for Diffraction Data. This is an Open Access article, distributed under the terms of the Creative Commons Attribution licence (<http://creativecommons.org/licenses/by/4.0>), which permits unrestricted re-use, distribution and reproduction, provided the original article is properly cited. [doi:10.1017/S0885715625101061]

Key words: fluvoxamine, Luvox[®], crystal structure, Rietveld refinement, density functional theory

I. INTRODUCTION

Fluvoxamine maleate (sold under the brand names Luvox[®] and Faverin[®], among others) is an antidepressant, used to treat major depressive disorder and obsessive-compulsive disorder, but is also used to treat other mental disorders, including anxiety, panic, social anxiety, and post-traumatic stress. The systematic name (CAS Registry Number 61718-82-9) is 2-[(E)-[5-methoxy-1-[4-(trifluoromethyl)phenyl]pentylidene]amino]oxyethan ammonium hydrogen (Z)-but-2-enedioate. Conventional naming is fluvoxamine maleate, though it is a 1:1 salt and is more correctly named fluvoxamine hydrogen maleate. A two-dimensional molecular diagram of fluvoxamine hydrogen maleate is shown in Figure 1.

A powder diffraction pattern for fluvoxamine maleate from a flat plate specimen on a Philips diffractometer is reported by Foda et al. (1996), along with other chemical and physical data. Differential scanning calorimetry (DSC) and X-ray diffraction results indicated the presence of polymorphism, but infrared spectroscopy (IR) spectra were less clear. The Foda et al. (1996) powder pattern is limited, missing the low-angle portion (Figure 2). It is not completely clear that the patterns represent the same material. Our synchrotron pattern seems to contain additional peaks, so it may represent a mixture.

This work was carried out as part of a project (Kaduk et al., 2014) to determine the crystal structures of large-volume commercial pharmaceuticals and include high-quality powder diffraction data for them in the Powder Diffraction File (Kabekkodu et al., 2024).

II. EXPERIMENTAL

Commercial reagent fluvoxamine maleate was purchased from TargetMol (Batch #T1077) and was used as-received. The white powder was packed into a 0.5-mm-diameter Kapton capillary and rotated during the measurement at ~2 Hz. The powder pattern was measured at 298(1) K at the Wiggler Low Energy Beamline (Leontowich et al., 2021) of the Brookhouse X-ray Diffraction and Scattering Sector of the Canadian Light Source using a wavelength of 0.819826(2) Å (15.1 keV) from 1.6 to 75.0° 2 θ with a step size of 0.0025° and a collection time of 3 minutes. The high-resolution powder diffraction data were collected using eight Dectris Mythen2 X series 1K linear strip detectors. NIST SRM 660b LaB₆ was used to calibrate the instrument and refine the monochromatic wavelength used in the experiment.

The pattern was difficult to index. DICVOL06 (Louër and Boulton, 2007) as incorporated into EXPO2014 (Altomare et al., 2013) yielded a cell with a reasonable (integral number of formula units) volume only when up to three unindexed lines were permitted. This primitive monoclinic cell had $a = 21.6506$, $b = 5.3443$, $c = 19.5852$ Å, $\beta = 100.071^\circ$, $V = 2,231.5$ Å³, and $Z = 4$. A reduced cell search of the Cambridge Structural Database (Groom et al., 2016) yielded four hits, but no structures of fluvoxamine or its derivatives.

This cell does not account for all of the peaks in the pattern. Other indexing programs suggested larger cells ($Z = 8$ or 16), but they did not yield chemically reasonable crystal structures, particularly where one expects to observe N–H...O cation–anion hydrogen bonds. We examined the 2 \times supercells calculated by NBS*LATTICE (Karen and Mighell, 1985). A triclinic supercell with $a = 10.674$, $b = 20.304$, $c = 22.320$ Å, $\alpha = 76.86^\circ$, $\beta = 76.17^\circ$, and $\gamma = 74.76^\circ$ yielded the best LeBail fit among the seven supercells, and was roughly similar to a triclinic cell

Corresponding author: James Kaduk; Email: kaduk@polycrystallography.com

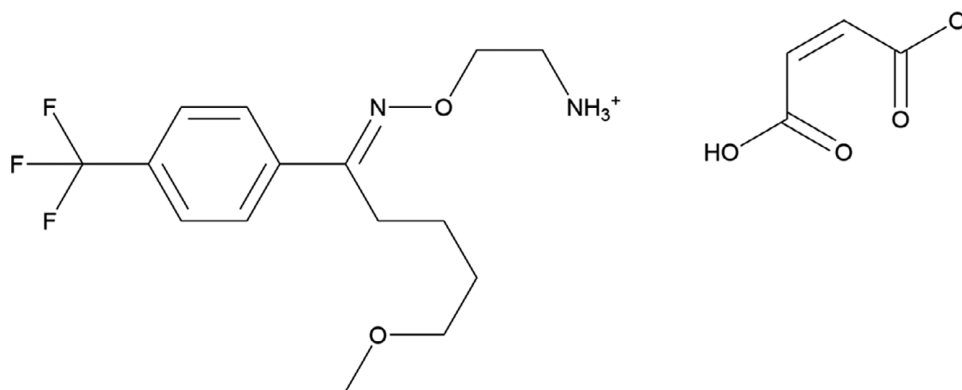


Figure 1. The two-dimensional structure of fluvoxamine hydrogen maleate.

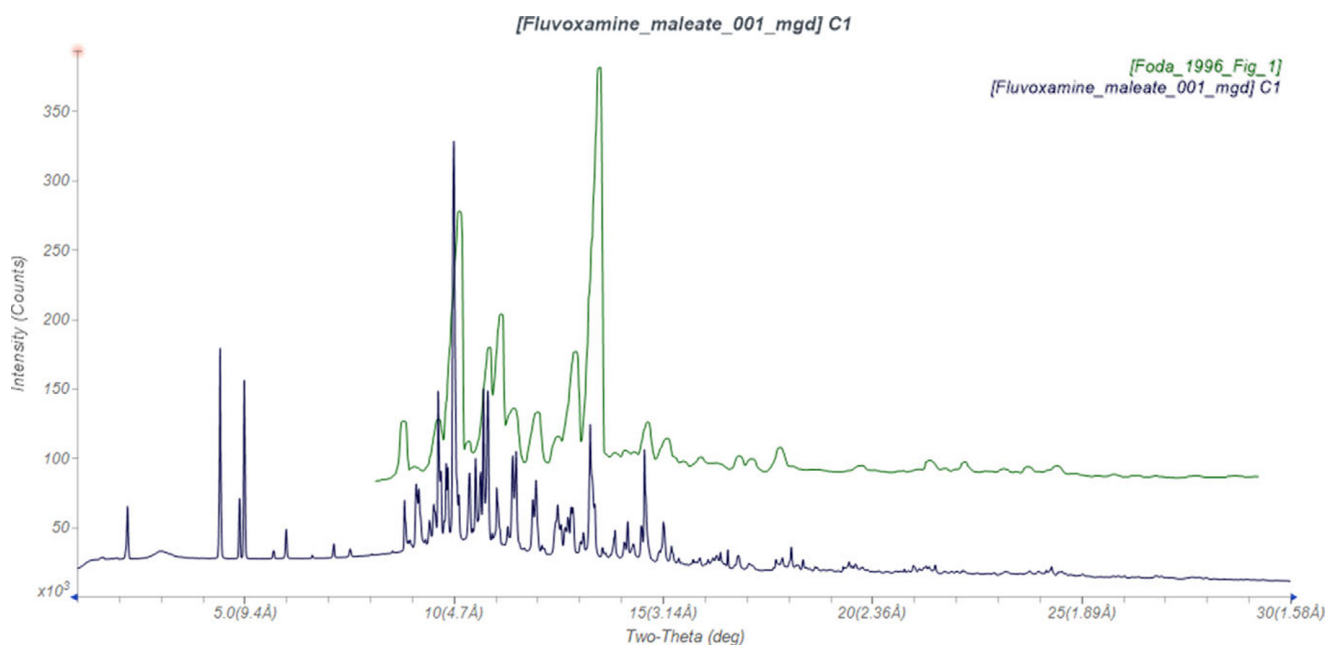


Figure 2. Comparison of the synchrotron pattern of fluvoxamine maleate (black) to that reported by Foda et al. (1996) (green). The Foda et al. (1996) pattern (measured using Cu K_{α} radiation) was digitized using UN-SCAN-IT (Silk Scientific, 2013) and converted to the synchrotron wavelength of 0.819826(2) Å using JADE Pro (MDI, 2024). Image generated using JADE Pro (MDI, 2024).

suggested by some indexing programs. Using the transformation matrices reported by NBS*LATTICE, the monoclinic cell was transformed into this $2 \times$ triclinic cell. The monoclinic structure (see below) was transformed into the triclinic $P-1$ cell using Materials Studio (Dassault Systèmes, 2024). Although a slightly better fit to the pattern was obtained, the bonds and angles deviated widely from normal values. This doubled cell model was found to be a false path.

A fluvoxamine molecular structure was downloaded from PubChem (Kim et al., 2023) as Conformer3D_COMP OUND_CID_5324396.sdf. It was converted to a *.mol2 file using Mercury (Macrae et al., 2020). The additional hydrogen atom was added to the amino group using Materials Studio to create the cation. The structure of a maleate anion was extracted from that of rosiglitazone maleate hydrate (CSD Refcode KIWVUI; Cuffini et al., 2008). The structure was solved by Monte Carlo-simulated annealing techniques as implemented in EXPO2014 (Altomare et al., 2013), using the cation ($-\text{NH}_3^+$) and anion ($-\text{O}^-$) as fragments and

including a bump penalty. The suggested space group was $P2_1/c$, which was confirmed by the successful solution and refinement of the structure. The torsion angles of the anion were fixed, making it a rigid body.

Rietveld refinement was carried out with GSAS-II (Toby and Von Dreele, 2013). Only the $1.5\text{--}45.0^\circ$ portion of the pattern was included in the refinements ($d_{\min} = 1.071 \text{ Å}$). All non-H-bond distances and angles were subjected to restraints, based on a Mercury/Mogul Geometry Check (Bruno et al., 2004; Sykes et al., 2011). The Mogul average and standard deviation for each quantity were used as the restraint parameters. The aromatic ring system in the cation was restrained to be planar. The restraints contributed 5.7% to the overall χ^2 . Lowering the restraint weights resulted in an unreasonable geometry (long C–C bonds in the side chains of the cation). The hydrogen atoms were included in calculated positions, which were recalculated during the refinement using Materials Studio (Dassault Systèmes, 2024). The U_{iso} of the heavy atoms were grouped by chemical similarity.

Attempts to refine the displacement coefficients led to very large values (0.3–0.5 Å²), so they were fixed at reasonable values, at the cost of slightly higher residuals. The high U_{iso} values suggested possible disorder in the trifluoromethyl groups and the side chains, but since an ordered model is necessary for the density functional theory (DFT) calculations, we chose not to model any disorder. The peak profiles were described using a uniaxial microstrain model, with [010] as the unique axis, based on the anisotropy of the lattice parameters. The background was modeled using a six-term shifted Chebyshev polynomial, with peaks at 3.03 and 11.23° 2θ to model the narrow and broad scattering from the Kapton capillary and any amorphous component of the sample.

The final refinement of 118 variables using 17,401 observations and 66 restraints yielded the residual $R_{\text{wp}} = 0.11279$. The largest peak (0.94 Å from F1) and hole (1.41 Å from F1) in the difference Fourier map were 0.74(17) and −0.75(17) eÅ^{−3}, respectively. The final Rietveld plot is shown in Figure 3. The largest features in the normalized error plot are in the shapes, positions, and intensities of some of the strong low-angle peaks, as well as at weaker higher-angle peaks, and the unindexed peaks. The sample seems to contain at least one additional crystalline phase and has probably changed during the measurement.

The crystal structure of fluvoxamine maleate was optimized (fixed experimental unit cell) with density functional theory techniques using VASP (Kresse and Furthmüller, 1996) through the MedeA graphical interface (Materials Design, 2024). The calculation was carried out on 32 cores of a 144-core (768 GB memory) HPE Superdome Flex 280 Linux server at North Central College. The calculation used the GGA-PBE functional, a plane-wave cutoff energy of 400.0 eV, and a k -point spacing of 0.5 Å^{−1}, leading to a 1 × 3 × 1 mesh, and took ~31.0 hours. Structure optimization and population analysis density functional theory calculations (fixed experimental cell) were carried out using

CRYSTAL23 (Erba et al., 2023). The basis sets for the H, C, N, and O atoms in the calculation were those of Gatti et al. (1994), and that for F was that of Peintinger et al. (2013). The calculations were run on a 3.5 GHz PC using eight k -points and the B3LYP functional, and took ~18.7 days.

III. RESULTS AND DISCUSSION

The sample of fluvoxamine maleate studied here appears to be a mixture and has probably suffered some beam damage. We propose a chemically reasonable crystal structure (with the expected features), which is consistent with the DFT optimizations. It should serve for the purposes of phase identification and quantitative phase analysis until a better sample can be characterized.

The availability of computer time permitted separate DFT geometry optimizations of the crystal structure of fluvoxamine maleate using both CRYSTAL23 and VASP. The structures differ significantly. The root-mean-square (rms) difference of the non-H atoms in the two optimized structures, calculated using the Mercury CSD-Materials/Search/Crystal Packing Similarity tool, is 0.454 Å (Table I and Figure 4). The rms Cartesian displacements of the non-H atoms in the optimized structures of the cation, calculated using the Mercury

TABLE I. Root-mean-square Cartesian displacements of non-H atoms in fluvoxamine maleate.

	GSAS	CRYSTAL23	VASP
GSAS	–	0.535	0.595
		0.365	0.359
CRYSTAL23	0.637	–	0.402
			0.043
VASP	0.637	0.454	–

Top/right = molecule overlay; top = cation, bottom = anion; bottom/left = crystal packing similarity.

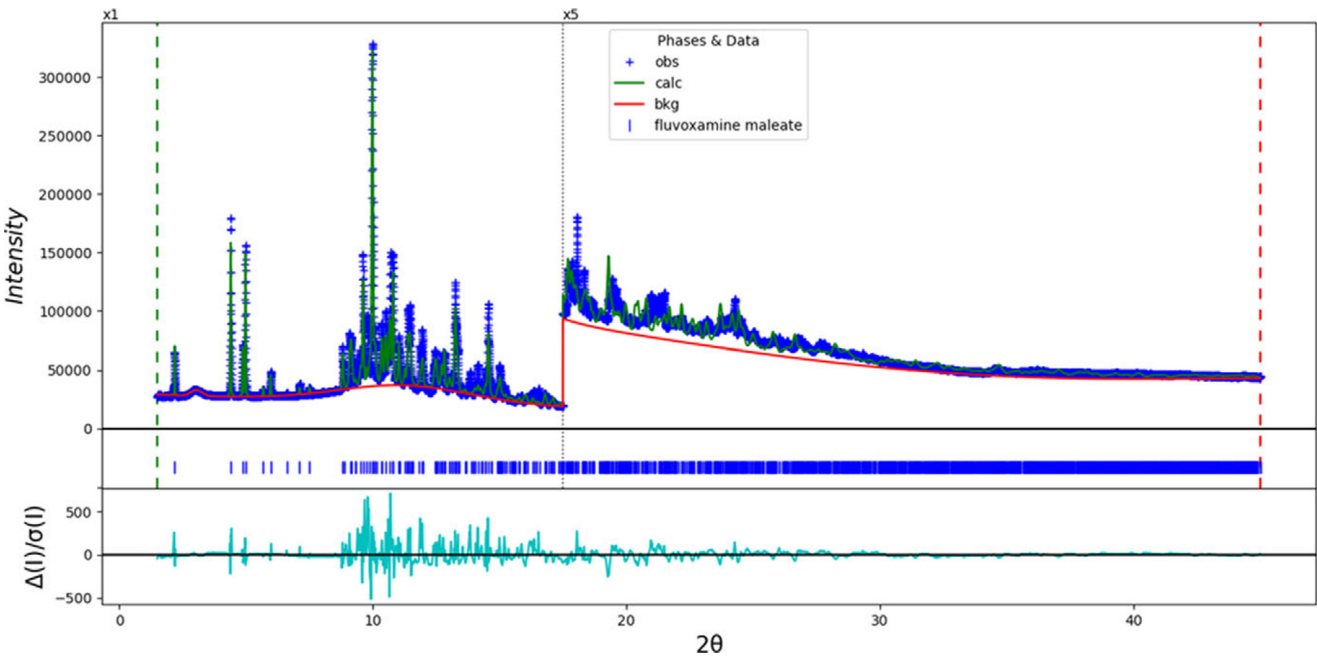


Figure 3. The Rietveld plot for fluvoxamine maleate. The blue crosses represent the observed data points, and the green line is the calculated pattern. The cyan curve is the normalized error plot, and the red line is the background curve. The blue tick marks indicate the fluvoxamine maleate peak positions. The vertical scale has been multiplied by a factor of 5× for 2θ > 17.5.

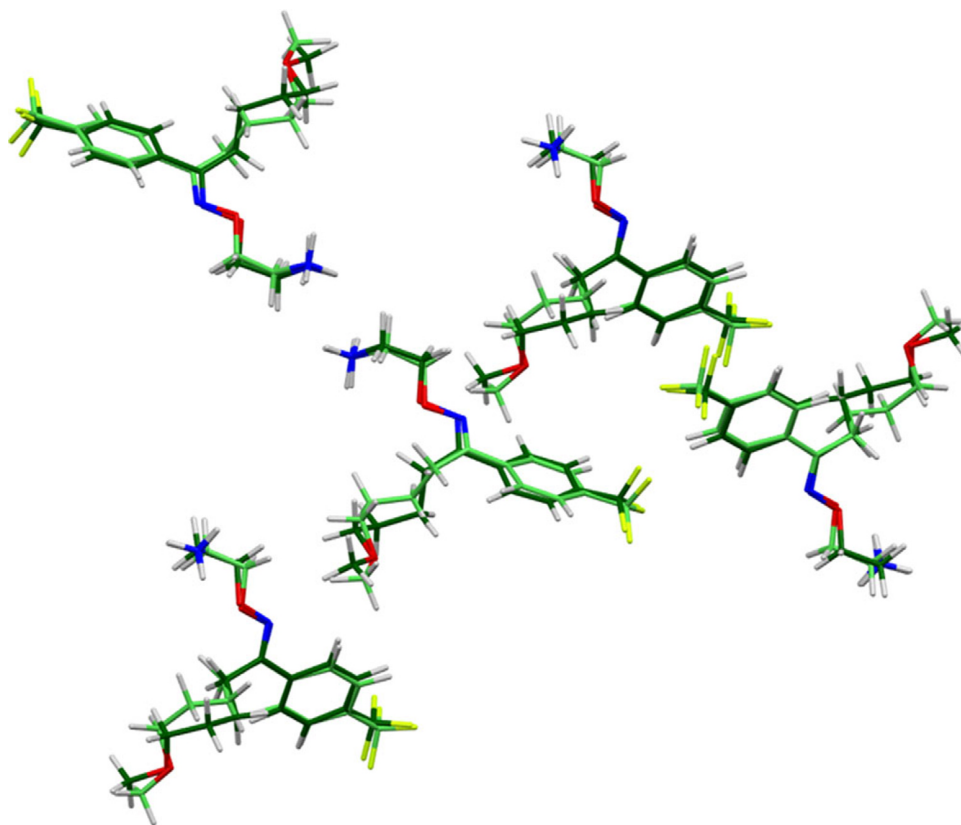


Figure 4. Comparison of the CRYSTAL23-optimized structure of fluvoxamine maleate (colored by atom type) to the VASP-optimized structure (green). The comparison was generated by the Mercury CSD-Materials/Search/Crystal Packing Similarity tool; the root-mean-square displacement is 0.454 Å. Image generated using Mercury (Macrae et al., 2020).

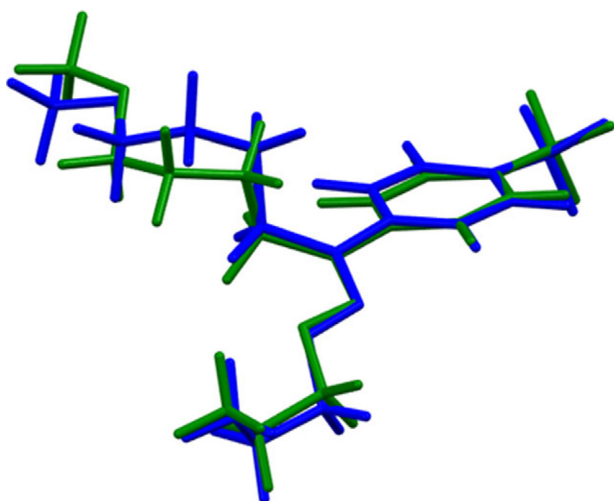


Figure 5. Comparison of the CRYSTAL23-optimized structure of the fluvoxamine cation (blue) to the VASP-optimized structure (green). The comparison was generated using the Mercury Calculate/Molecule Overlay tool; the root-mean-square difference is 0.402 Å. Image generated using Mercury (Macrae et al., 2020).

Calculate/Molecule Overlay tool, are 0.402 Å (Table I). The main differences are in the conformation of the methoxybutyl side chain (Figure 5). The difference in the optimized anions is much smaller at 0.043 Å (Figure 6). It is noteworthy that CRYSTAL23 yields a more asymmetric intramolecular O–H...O hydrogen bond in the maleate anion (O–H = 1.054

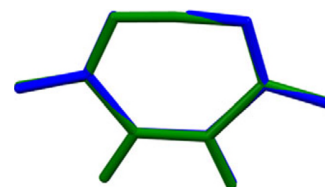


Figure 6. Comparison of the CRYSTAL23-optimized structure of the hydrogen maleate anion (blue) to the VASP-optimized structure (green). The comparison was generated using the Mercury Calculate/Molecule Overlay tool; the root-mean-square difference is 0.043 Å. Image generated using Mercury (Macrae et al., 2020).

and 1.402 Å) than does VASP (1.111 and 1.322 Å). These results demonstrate that the results of a DFT optimization also contain some uncertainty. Because we analyze the hydrogen bonds using the CRYSTAL23 results, we will emphasize that structure in the remaining discussion.

The rms difference of the non-H atoms in the Rietveld-refined and CRYSTAL23-optimized structures, calculated using the Mercury CSD-Materials/Search/Crystal Packing Similarity tool, is 0.637 Å (Table I). The rms Cartesian displacements of the non-H atoms in the Rietveld-refined and CRYSTAL23-optimized structures of the cation and anion, calculated using the Mercury Calculate/Molecule Overlay tool, are 0.535 and 0.365 Å (Figure 7). The agreements are outside the normal range for correct structures (van de Streek and Neumann, 2014). The main differences in the cation lie in the side chains. The maleate anion in the refined

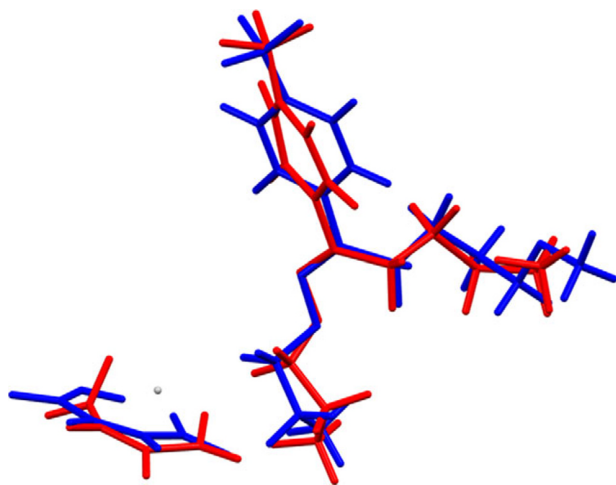


Figure 7. Comparison of the Rietveld-refined (red) and CRYSTAL23-optimized (blue) structures of fluvoxamine hydrogen maleate. The root-mean-square differences are 0.535 and 0.365 Å for the cation and the anion, respectively. Image generated using Mercury (Macrae et al., 2020).

structure differs considerably from the expected planar conformation (Figure 8), and is chemically unreasonable. Correlations among variables almost certainly propagate this unreasonableness to the cation. Since this organic compound was measured on a wiggler beamline, the specimen almost certainly changed during the measurement, making the experimental structure less reliable than might be desired. We believe that the optimized structure is reliable. The asymmetric unit is illustrated in Figure 9.

All of the bond distances and bond angles, and most of the torsion angles, fall within the normal ranges indicated by a Mercury Mogul Geometry check (Macrae et al., 2020). The C11–C9–C8–C10 torsion angle of -145.5° lies on the tail of the major *trans* fraction of a *trans/gauche* distribution of similar torsion angles. The C12–C11–C9–C8 torsion angle of -56.6° lies on the tail of a distribution. The conformation of the cation is slightly unusual.

Quantum chemical geometry optimization of an isolated fluvoxamine cation (DFT/B3LYP/6-31G*/water) using Spartan'24 (Wavefunction, 2023) indicated that the observed conformation is 6.7 kcal/mol higher in energy than the local minimum, which has a different conformation of the methoxybutyl chain. The global minimum-energy conformation is more compact (folded on itself), indicating that intermolecular interactions are important in determining the solid-state conformation.

The crystal structure (Figure 10) consists of alternating double layers of cations and anions parallel to the *bc*-plane. The trifluoromethyl groups are adjacent to each other.

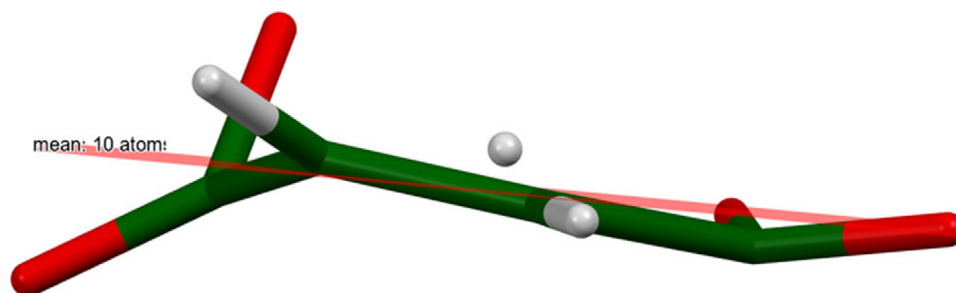


Figure 8. The deviation of the refined structure of the hydrogen maleate anion from the mean plane. Image generated using Mercury (Macrae et al., 2020).

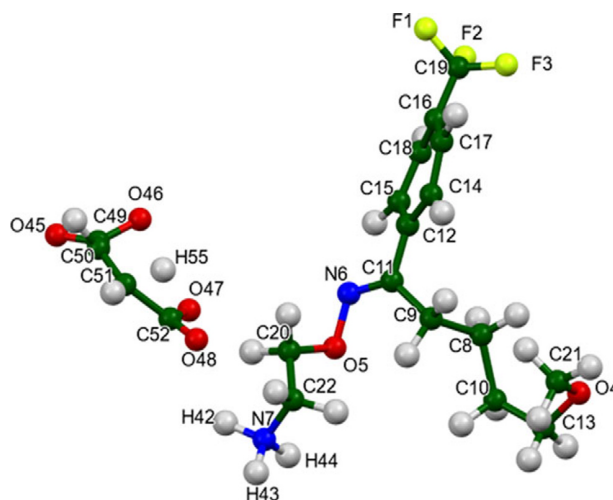


Figure 9. The experimental asymmetric unit of fluvoxamine hydrogen maleate, with the atom numbering. The atoms are represented by 50% probability spheroids. Image generated using Mercury (Macrae et al., 2020).

Hydrogen bonds (discussed below) link the layers of anions and cations parallel to the *bc*-plane. The Mercury Aromatics Analyser indicates only a weak interaction between the phenyl rings, with a distance of 9.87 Å.

As expected, each of the three protons in the ammonium group N7 acts as a donor in a strong N–H \cdots O hydrogen bond to the anion (Table II). The charge on O48 is larger than that on O45 (-0.59 vs. 0.49), making it reasonable that it is an acceptor in two hydrogen bonds. H44 also participates in a weaker intramolecular N–H \cdots O hydrogen bond. The energies of the N–H \cdots O hydrogen bonds were calculated using the correlation of Wheatley and Kaduk (2019). Intramolecular C–H \cdots O and C–H \cdots N hydrogen bonds, as well as an intermolecular C–H \cdots O hydrogen bond between the cation and anion, also contribute to the crystal energy. As expected, there is a very strong O–H \cdots O hydrogen bond in the hydrogen maleate anion. The energy of this hydrogen bond was calculated using the correlation of Rammohan and Kaduk (2018). There are also C–H \cdots O hydrogen bonds between the maleate anions. The N–H \cdots O hydrogen bonds between the cations and the anions link them in a two-dimensional layer parallel to the *bc*-plane (Figure 11). Prominent in these layers are rings with a graph set *R2,4(8)* (Etter, 1990; Bernstein et al., 1995; Motherwell et al., 2000) and chains with graph set *C2,2(9)*.

The volume enclosed by the Hirshfeld surface of fluvoxamine maleate (Figure 12; Hirshfeld, 1977; Spackman et al., 2021) is 544.40 Å³, 98.26% of one-fourth of the unit cell volume. The packing density is thus typical. The only

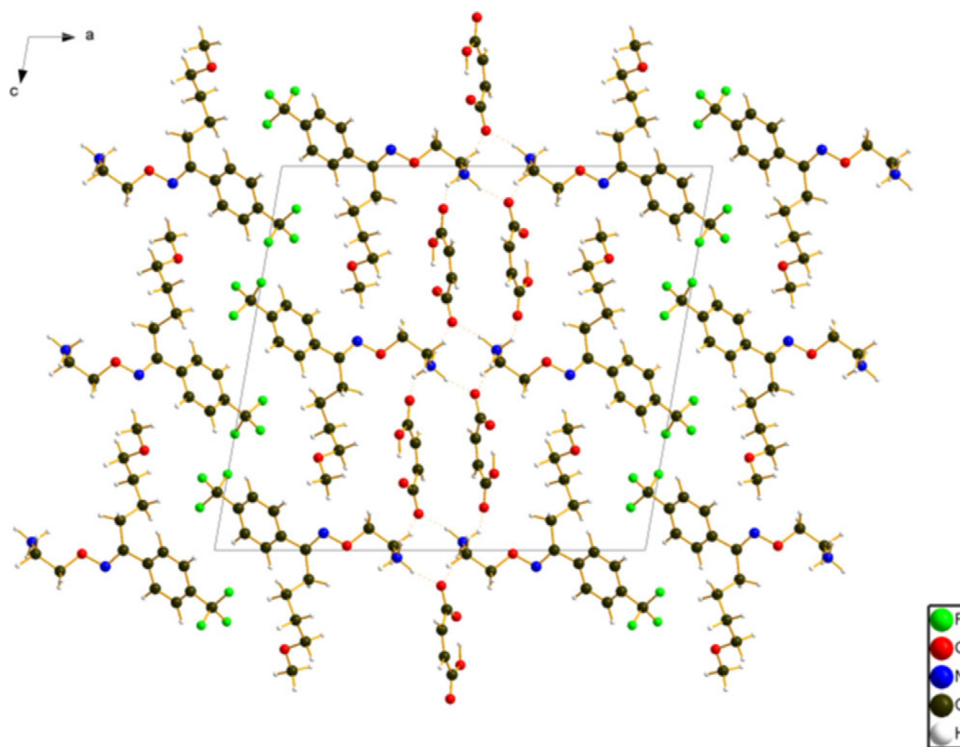


Figure 10. The VASP-optimized crystal structure of fluvoxamine hydrogen maleate, viewed down the *b*-axis. Image generated using Diamond (Crystal Impact, 2023).

TABLE II. Hydrogen bonds (CRYSTAL23) in fluvoxamine maleate.

H bond	D–H, Å	H···A, Å	D···A, Å	D–H···A, °	Mulliken overlap, <i>e</i>	<i>E</i> , kcal/mol
N7–H42···O48	1.036	1.782	2.758	155.2	0.062	5.8
N7–H43···O48	1.042	1.729	2.720	157.2	0.078	6.4
N7–H44···O45	1.034	1.894	2.709	133.1	0.050	5.2
N7–H44···O5	1.034	2.534*	2.828	95.5	0.015	2.8
C9–H26···O5	1.090	2.203*	2.704	105.3	0.018	
C15–H32···N6	1.084	2.516*	2.764	91.4	0.010	
C22–H41···O45	1.091	2.240	3.303	164.3	0.031	
O46–H55···O47	1.054	1.402*	2.452	172.9	0.103	17.5
C50–H53···O46	1.084	2.368	3.193	131.6	0.017	
C51–H54···O47	1.086	2.407	3.278	136.2	0.018	

*Intramolecular.

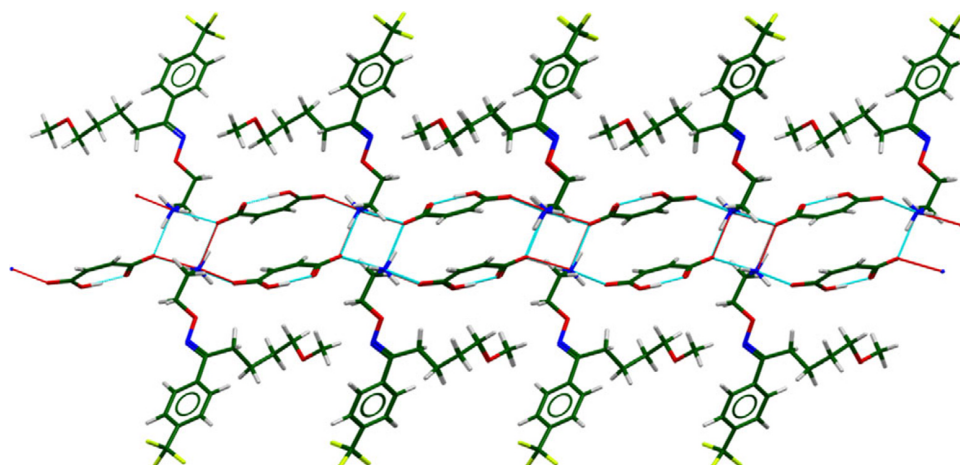


Figure 11. The hydrogen-bonded layers in the crystal structure of fluvoxamine hydrogen maleate. The *bc*-plane is horizontal. Image generated using Mercury (Macrae et al., 2020).

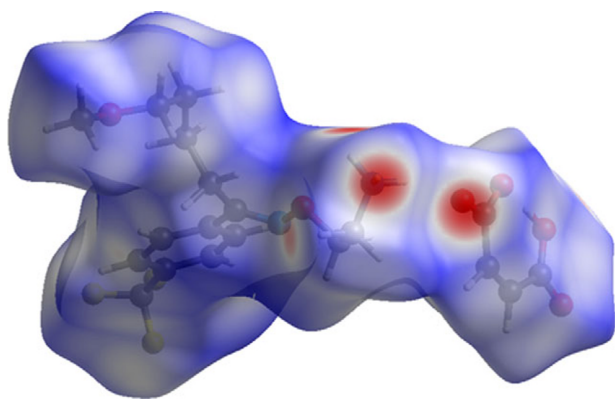


Figure 12. The Hirshfeld surface of fluvoxamine hydrogen maleate. Intermolecular contacts longer than the sum of the van der Waals radii are colored blue, and contacts shorter than the sum of the radii are colored red. Contacts equal to the sum of radii are white. Image generated using CrystalExplorer (Spackman et al., 2021).

significant close contacts (red in Figure 12) involve the hydrogen bonds. The volume/non-hydrogen atom is slightly larger than usual at 18.5 \AA^3 .

The Bravais–Friedel–Donnay–Harker (Bravais, 1866; Friedel, 1907; Donnay and Harker, 1937) algorithm suggests that we might expect platy morphology for fluvoxamine maleate, with {100} as the major faces. A fourth-order spherical harmonic model was included in the refinement. The texture index was 1.109(6), indicating that the preferred orientation was significant in this rotated capillary specimen.

DEPOSITED DATA

The powder pattern of fluvoxamine hydrogen maleate from this synchrotron dataset has been submitted to the International Centre for Diffraction Data (ICDD) for inclusion in the Powder Diffraction File. The Crystallographic Information Framework (CIF) files containing the results of the Rietveld refinement (including the raw data) and the DFT geometry optimization were deposited with the ICDD. The data can be requested at pdj@icdd.com.

ACKNOWLEDGEMENTS

We thank Adam Leontowich for his assistance in the data collection. We also thank the ICDD team – Megan Rost, Steve Trimble, and Dave Bohnenberger – for their contribution to research, sample preparation, and in-house XRD data collection and verification.

FUNDING STATEMENT

Part of the research described in this paper was performed at the Canadian Light Source, a national research facility of the University of Saskatchewan, which is supported by the Canada Foundation for Innovation (CFI), the Natural Sciences and Engineering Research Council (NSERC), the Canadian Institute of Health Research (CIHR), the Government of Saskatchewan, and the University of Saskatchewan. This work was partially supported by the International Centre for Diffraction Data.

COMPETING INTERESTS

The authors have no competing interests.

REFERENCES

- Altomare, A., C. Cuocci, C. Giacovazzo, A. Moliterni, R. Rizzi, N. Corriero, and A. Falcicchio. 2013. “EXPO2013: A Kit of Tools for Phasing Crystal Structures from Powder Data.” *Journal of Applied Crystallography* 46: 1231–35.
- Bernstein, J., R. E. Davis, L. Shimoni, and N. L. Chang. 1995. “Patterns in Hydrogen Bonding: Functionality and Graph Set Analysis in Crystals.” *Angewandte Chemie International Edition in English* 34: 1555–73.
- Bravais, A. 1866. *Etudes Cristallographiques*. Paris: Gauthier Villars.
- Bruno, I. J., J. C. Cole, M. Kessler, J. Luo, W. D. S. Motherwell, L. H. Purkis, B. R. Smith, et al. 2004. “Retrieval of Crystallographically Derived Molecular Geometry Information.” *Journal of Chemical Information and Computer Sciences* 44: 2133–44.
- Crystal Impact. 2023. *Diamond V. 5.0.0*. Bonn: Crystal Impact – Dr. H. Putz & Dr. K. Brandenburg.
- Cuffini, S. L., S. Faudone, M. Ferro, M. T. Garland, and R. Baggio. 2008. “Rosiglitazone Maleate 0.25-Hydrate: A Pseudopolymorphic Form.” *Acta Crystallographica Section C: Crystal Structure Communications* 64: o119–o122. <https://doi.org/10.1107/S0108270107054443>.
- Dassault Systèmes. 2024. *BIOVIA Materials Studio 2025*. San Diego, CA: BIOVIA.
- Donnay, J. D. H., and D. Harker. 1937. “A New Law of Crystal Morphology Extending the Law of Bravais.” *American Mineralogist* 22: 446–67.
- Erba, A., J. K. Desmarais, S. Casassa, B. Civalleri, L. Donà, I. J. Bush, B. Searle, et al. 2023. “CRYSTAL23: A Program for Computational Solid State Physics and Chemistry.” *Journal of Chemical Theory and Computation* 19: 6891–932. <https://doi.org/10.1021/acs.jctc.2c00958>.
- Etter, M. C. 1990. “Encoding and Decoding Hydrogen-Bond Patterns of Organic Compounds.” *Accounts of Chemical Research* 23: 120–26.
- Foda, N. H., M. A. Radwan, and O. A. Al Deeb. 1996. “Fluvoxamine Maleate.” *Analytical Profiles of Drug Substances and Excipients* 24: 165–208.
- Friedel, G. 1907. “Etudes sur la loi de Bravais.” *Bulletin de la Société Française de Minéralogie* 30: 326–455.
- Gatti, C., V. R. Saunders, and C. Roetti. 1994. “Crystal-Field Effects on the Topological Properties of the Electron-Density in Molecular Crystals – the Case of Urea.” *Journal of Chemical Physics* 101: 10686–96.
- Groom, C. R., I. J. Bruno, M. P. Lightfoot, and S. C. Ward. 2016. “The Cambridge Structural Database.” *Acta Crystallographica Section B: Structural Science, Crystal Engineering and Materials* 72: 171–79.
- Hirshfeld, F. L. 1977. “Bonded-Atom Fragments for Describing Molecular Charge Densities.” *Theoretica Chimica Acta* 44: 129–38.
- Kabekkodu, S., A. Dosen, and T. N. Blanton. 2024. “PDF-5+: A Comprehensive Powder Diffraction File™ for Materials Characterization.” *Powder Diffraction* 39: 47–59.
- Kaduk, J. A., C. E. Crowder, K. Zhong, T. G. Fawcett, and M. R. Suchomel. 2014. “Crystal Structure of Atomoxetine Hydrochloride (Strattera), C₁₇H₂₃NOCl.” *Powder Diffraction* 29: 269–73.
- Karen, V. L., and A. D. Mighell. 1985. “NBS* LATTICE: A Program to Analyze Lattice Relationships.” National Bureau of Standards (US) Technical Note 1214.
- Kim, S., J. Chen, T. Cheng, A. Gindulyte, J. He, S. He, Q. Li, et al. 2023. “PubChem 2023 Update.” *Nucleic Acids Research* 51 (D1): D1373–80. <https://doi.org/10.1093/nar/gkac956>.
- Kresse, G., and J. Furthmüller. 1996. “Efficiency of Ab-Initio Total Energy Calculations for Metals and Semiconductors Using a Plane-Wave Basis Set.” *Computational Materials Science* 6: 15–50.
- Leontowich, A. F. G., A. Gomez, B. Diaz Moreno, D. Muir, D. Spasyuk, G. King, J. W. Reid, C.-Y. Kim, and S. Kycia. 2021. “The Lower Energy Diffraction and Scattering Side-Bounce Beamline for Materials Science at the Canadian Light Source.” *Journal of Synchrotron Radiation* 28: 961–69.
- Louër, D., and A. Boulton. 2007. “Powder Pattern Indexing and the Dichotomy Algorithm.” *Zeitschrift für Kristallographie Supplement* 26: 191–96.

- Macrae, C. F., I. Sovago, S. J. Cottrell, P. T. A. Galek, P. McCabe, E. Pidcock, M. Platings, et al. 2020. "Mercury 4.0: From Visualization to Design and Prediction." *Journal of Applied Crystallography* 53: 226–35.
- Materials Design. 2024. *MedeA 3.7.2*. San Diego, CA: Materials Design, Inc.
- MDI. 2024. *JADE Pro Version 9.0*. Livermore, CA: Materials Data.
- Motherwell, W. D. S., G. P. Shields, and F. H. Allen. 2000. "Graph-Set and Packing Analysis of Hydrogen-Bonded Networks in Polyamide Structures in the Cambridge Structural Database." *Acta Crystallographica B* 56: 857–71.
- Peintinger, M. F., D. Vilela Oliveira, and T. Bredow. 2013. "Consistent Gaussian Basis Sets of Triple-Zeta Valence with Polarization Quality for Solid-State Calculations." *Journal of Computational Chemistry* 34: 451–59.
- Rammohan, A., and J. A. Kaduk. 2018. "Crystal Structures of Alkali Metal (Group 1) Citrate Salts." *Acta Crystallographica Section B: Crystal Engineering and Materials* 74: 239–52.
- Silk Scientific. 2013. *UN-SCAN-IT 7.0*. Orem, UT: Silk Scientific Corporation.
- Spackman, P. R., M. J. Turner, J. J. McKinnon, S. K. Wolff, D. J. Grimwood, D. Jayatilaka, and M. A. Spackman. 2021. "CrystalExplorer: A Program for Hirshfeld Surface Analysis, Visualization and Quantitative Analysis of Molecular Crystals." *Journal of Applied Crystallography* 54: 1006–11. <https://doi.org/10.1107/S1600576721002910>.
- Sykes, R. A., P. McCabe, F. H. Allen, G. M. Battle, I. J. Bruno, and P. A. Wood. 2011. "New Software for Statistical Analysis of Cambridge Structural Database Data." *Journal of Applied Crystallography* 44: 882–86.
- Toby, B. H., and R. B. Von Dreele. 2013. "GSAS II: The Genesis of a Modern Open Source All Purpose Crystallography Software Package." *Journal of Applied Crystallography* 46: 544–49.
- van de Streek, J., and M. A. Neumann. 2014. "Validation of Molecular Crystal Structures from Powder Diffraction Data with Dispersion-Corrected Density Functional Theory (DFT-D)." *Acta Crystallographica Section B: Structural Science, Crystal Engineering and Materials* 70: 1020–32.
- Wavefunction, Inc. 2023. *Spartan'24. V. 1.0.0*. Irvine, CA: Wavefunction, Inc.
- Wheatley, A. M., and J. A. Kaduk. 2019. "Crystal Structures of Ammonium Citrates." *Powder Diffraction* 34: 35–43.